Journal of Science and Technology in Civil Engineering, HUCE, 2024, 18 (1): 153–163

A COMPARATIVE STUDY OF TWO CORRELATION FUNCTIONS APPLYING TO THE QUANTITATIVE CHARACTERIZATION OF THE PORE STRUCTURE WITHIN HARDENED CONCRETE

Vu Chi Cong[a,*]

[a]*Faculty of Building and Industrial Construction, Hanoi University of Civil Engineering, 55 Giai Phong road, Hai Ba Trung district, Hanoi, Vietnam*

Article history:
Received 08/01/2024, Revised 23/02/2024, Accepted 26/02/2024

Abstract

The paper presents a comparative study between the autocorrelation function (ACF) and the 2-point correlation function (2PCF) for the quantitative analysis of the pore structure within hardened concrete via the image analysis technique. This work was carried out on five cross-sectional images of concrete specimens with varying area porosities ranging from 2.6% to 21.2%. This research indicates that: (i) the ACF provides a comprehensive and effective tool that is capable of capturing the contribution of the area porosity, size, and orientation of the pores in quantifying the pore structure within hardened concrete, while the 2PCF only enables quantifying the size and spacing between the pores; (ii) the ACF requires the cross-sectional images to be square, whereas the 2PCF can analyze images of any size and shape; (iii) for an area porosity ($\phi_a \leq 20\%$), the characteristic size of the pore structure within hardened concrete, l_0, determined by both the ACF and 2PCF approaches, is not significantly different; (iv) on average, the correlation length (X_0) estimated by 2PCF is more than 1.6 times greater than the corresponding value determined by ACF; and (v) the characteristic size (l_0) provides a more accurate and comprehensive quantification of the pore structure within hardened concrete specimens than the correlation length (X_0).

Keywords: pore structure; image analysis; autocorrelation function; 2-point correlation function; characteristic size; correlation length.

https://doi.org/10.31814/stce.huce2024-18(1)-12

1. Introduction

Concrete is a typical heterogeneous material with various constitutive components (phases) such as coarse aggregates, cement-fine aggregate matrix, the interfacial transition zone (ITZ) between the cement paste and aggregates, and pores [1, 2]. Among these components, pore structures are often indicated to have a significant and direct influence on the variations in the mechanical properties and behaviors of hardened concrete under various types of loads [2–5]. The pores presented in the hardened concrete include three main components: capillary pores, gel pores, and air voids [2, 6]. According to Mehta and Monteiro [1], air voids, which typically appear in the cement-fine aggregate matrix with large sizes, have a primary influence on the mechanical behavior of concrete. On the other hand, the capillary pores and gel pores, which are much smaller in size (ranging from 0.5 nm to 1 μm), typically have little impact on the mechanical properties of concrete [7–9]. Therefore, when studying the influence of pore structures within hardened concrete on the mechanical properties of concrete, researchers primarily focus on the airvoids (hereinafter referred to as pores), and this is also the main focus of the present study.

*Corresponding author. *E-mail address:* congvc@huce.edu.vn (Cong, V. C.)

In terms of studying the pore structures within hardened concrete, besides traditional methods such as the liquid displacement method [5], mercury intrusion porosimetry [10–12], and the method of measuring alkali condensation [13, 14], digital image processing (DIP) and image analysis are increasingly being widely used due to their numerous advantages, especially in quantitative analysis. While traditional methods primarily assist in determining the apparent porosity and pore size distribution, DIP methods allow for a more extensive quantification of characteristic parameters of the pore structure, such as the apparent porosity, size, and shape of pores, the distance between pores, and the spatial distribution of pores within hardened concrete elements [15, 16].

In DIP and image analysis techniques, correlation functions are commonly employed as an effective tool for quantitatively analyzing the entire internal structure and/or specific constituent components of heterogeneous materials (e.g., concrete [17–20]). The fundamental principle of correlation functions in analyzing digital images is to calculate correlation values between corresponding pixels at different distances, thereby determining the characteristic size of the structure of the components presented in the image [17, 21]. This characteristic size can be regarded as the size of the Representative Volume Element (RVE) of the material in terms of microstructure and serves as an input parameter in numerical simulation analyses [22]. Two commonly used correlation functions in image analysis are the 2-point correlation function (2PCF) [17, 18, 20, 23] and the autocorrelation function (ACF) [24, 25]. For heterogeneous materials consisting of multiple phases, such as concrete or rock, ACF is primarily used on color images with structural components exhibiting various colors, whereas 2PCF can only be applied to binary images (i.e., the target phase appears white and the remaining phases are the black background). In terms of image analysis of the pore structures of concrete, as 2PCF does not require the image to be square-shaped, this function is more commonly employed than ACF. ACF is simpler mathematically and more visually intuitive compared to 2PCF since ACF values are represented in both directions of the image, while 2PCF is unidirectional [18, 21]. Nevertheless, until now, there has been no study comparing the results obtained from these two correlations in the quantitative analysis of the pore structures within hardened concrete.

This paper introduces a study comparing the results of quantitative analysis of the pore structures presented in hardened concrete using two correlation functions, ACF and 2PCF. This work mainly focuses on the comparison of the defined characteristic length of the pore structures and the correlation length derived from the ACF and 2PCF values. In addition, the influence of different features of the pore structures on the values of the characteristic size determined by these two correlation functions is also investigated.

2. Theoretical background

In image analysis, the digital image of a material cross-section is considered a matrix with dimensions of $M \times N$ pixels. Each pixel corresponds to a position (x, y) in the matrix with dimensions $M \times N$, where $x = 1 \rightarrow M$ and $y = 1 \rightarrow N$. The value $f(x, y)$ represents the color value at the pixel located at position (x, y). For binary images, the $f(x, y)$ value takes one of two values: 0 (for black color) and 1 (for white color) (see Fig. 1). In the following section, an overview of the autocorrelation function (ACF) and the 2-point correlation function (2PCF) will be presented.

2.1. Overview of the Autocorrelation Function

The autocorrelation function (ACF) is based on the self-correlation analysis of a dataset with the same dataset. In image analysis, the ACF of an image is essentially the self-correlation analysis (or repeated convolution) of the color values at the pixels in that image, as expressed in Eq. (1) below:

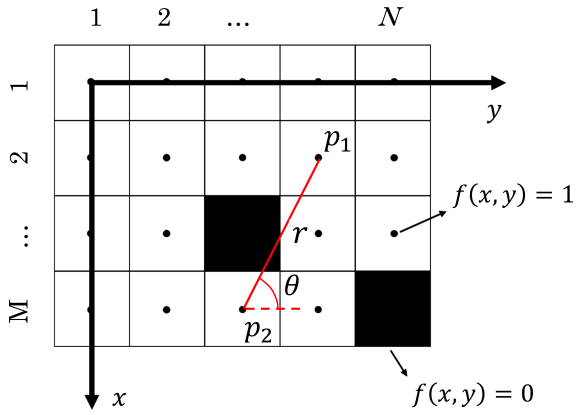

Figure 1. Illustration of the matrix of pixels for a binary image with dimensions of $M \times N$ pixels ([18])

$$f(x,y) \otimes f(x,y) = \int_{-\infty}^{+\infty}\int_{-\infty}^{+\infty} f(x',y')f(x+x',y+y')dx'dy' \tag{1}$$

where $f(x,y)$ represents the color value at the point with coordinates (x,y) in the image, $\otimes$ denotes the convolution operator, (x',y') refers to the displacement distance of the image from its original position (x,y). For the application of the ACF, the Fast Fourier Transforms (FFT) are commonly employed. Hence, the image must be square. In other words, the matrix of pixels must be a square matrix with $M = N$ [21, 24, 25]. Applying the two-dimensional Fourier transform, the color value function $f(u,v)$ at the point with coordinates (u,v) is expressed as follows:

$$f(u,v) = \frac{1}{N}\sum_{x=0}^{N-1}\sum_{y=0}^{N-1} f(x,y)\exp[-2\pi i(ux+vy)] \tag{2}$$

where N is the size of the square matrix of pixels. The value of ACF at the point with coordinates (u,v) is determined by the product of $f\,(u,v)$ with its complex conjugate, $f^*\,(u,v)$. The matrix of ACF

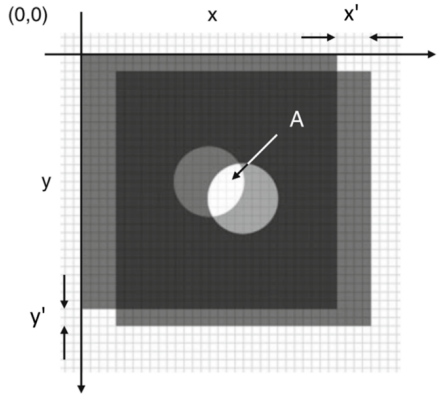

(a) Relative displacement (x',y') of a original image with its copy version, with A being the overlapping white region

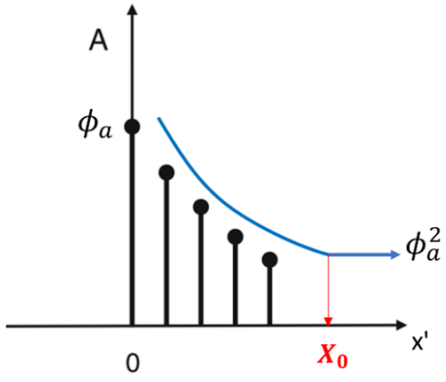

(b) Variation of the ACF value with the relative displacement $A\,(x')$

Figure 2. Illustration of the ACF analysis applied to an image of size $(x \times y)$ pixels with a white circle on a black background (modified from [21])

values is also a square matrix, and it has the same size as the matrix of the original pixels. According to [21, 26, 27], the ACF always achieves its maximum value at the center of the image, corresponding to the displacement $(x' = 0, y' = 0)$, and then gradually decreases towards the edges of the image as the values of (x', y') increase $(x' \to N/2, y' \to N/2)$. For binary images, the maximum value of the ACF is equal to ϕ_a, which represents the area ratio of the white region (see Fig. 2(a)). It then gradually decreases to the asymptotic value of ϕ_a^2 (see Fig. 2(b)) as the displacement (x', y') increases [20, 22].

2.2. *Overview of the two-point correlation function*

The 2-point correlation function (2PCF) refers to the probability of finding two points, p_1 and p_2, separated by a distance of r within the same phase (e.g., the same white phase as illustrated in Fig. 1) [19, 20, 28]. The correlation value between two points, p_1 and p_2, belonging to phase (i), $S_2(p_1, p_2)$, is determined by Eq. (3) below:

$$S_2^{(i)}(p_1, p_2) = S_2^{(i)}(p_{12}) = S_2^{(i)}(r) = \left\langle f(p_1)^{(i)} f(p_1 + r)^{(i)} \right\rangle \tag{3}$$

where $r = p_{12} = |p_2 - p_1|$ (see Fig. 1). If two points, p_1 and p_2, belong to phase (i), the value $f(p_{1,2}) = 1$. The two-point correlation value, S_2, is independent of the x and/or y direction and solely depends on the distance between the examined points [20]. In other words, the two-point correlation value can quantify the size and relative distance between components belonging to the same phase in the material structure. Similar to ACF, the two-point correlation value of a phase reaches its maximum value, $S_2 = \phi_a$, corresponding to the distance $r = 0$, then gradually decreases to the asymptotic value ϕ_a^2 as the distance increases $(r \to +\infty)$ [20, 28]. In the present work, the *"brute force"* method proposed by Berryman [29] and Velasquez [19] was employed to calculate the two-point correlation value, S_2. The principle of the "brute force"method is to estimate the value of S_2 for a given phase by calculating the ratio of the total number of pixels corresponding to that phase at a specific distance r, N_{r-hits}, to the total number of pixels in the analyzed image, N_{total}. Applying the above principle, in this study, the procedure for calculating the two-point correlation value, S_2, for the pore structures of hardened concrete is performed as follows:

+ Generate a random point, p_1, on the matrix of pixels with $f(p_1) = 1$;

+ Generate a point, p_2, at a distance of r from point p_1, randomly determined by an angle θ (see Fig. 1);

+ Calculate the total number of pixels, N_{r-hits}, where points p_2 are at a distance r from p_1 and both belong to the white phase $(f(p_2) = 1)$;

+ Calculate the two-point correlation value between points p_1 and p_2 at a distance r as $S_2(r, p_1, p_2) = \dfrac{N_{r-hits}}{N_{total}}$.

In this study, the generation of these random points is performed using the *rand()* function in the program MATLAB^{TM}.

2.3. *Characteristic size of the pore structure*

In terms of quantifying the microstructure via image analysis techniques, the distance corresponding to the position from which the correlation function value approaches a stable value is often used to indicate the value of the characteristic size of a material [19, 30, 31]. According to this definition, the distance corresponding to the position, X_0, commonly called the correlation length, where the correlation function (e.g., ACF or 2PCF) reaches the asymptotic value ϕ_a^2 (see Fig. 2(b)), can be regarded as the characteristic size of the pore structure. According to Kanit et al. [22, 30], the value of X_0 is often influenced by the largest size of the phase being analyzed (in the case of pore structures, X_0

would be directly related to the largest size of the pores). However, separating the boundaries of individual pores from the image (Fig. 3(c)) is challenging and requires complicated analysis algorithms. Moreover, considering only the maximum size of pores is just one factor to be considered when analyzing the pore structure of concrete. To indicate a characteristic size of the material structure in a general manner, Kanit et al. [22, 30] have introduced an integral range, l_0, estimated by the following equation:

$$l_0 = \frac{1}{C(0) - C(X_0)} \int_R [C(x) - C(X_0)]\, dx \tag{4}$$

where $C(x)$ is the value of the correlation function at a position with a distance of x. In this study, the value l_0 is used as the characteristic size of the pore structure of concrete.

3. Cross-sectional sample preparation

In general, the mix proportion and type of composition components of concrete are frequently found to be the important factors posibly influencing the pore structures within the hardened concrete [1, 2]. However, the pore structure and the porosity of hardened concrete are randomly stochastic properties. In other words, fabricating concrete samples with a predetermined mix proportion to achieve a pore structure within a hardened state with a given porosity is not feasible. On the other hand, to investigate the influence of the properties of the pore structure within hardened concrete on the effectiveness of its image analysis, a variety of images with different characteristics and porosities are required. Hence, in the present work, 05 (five) cross-sections of concrete samples available in the laboratory, fabricated from various mixtures, were used for analysis. The sample cross-sections were ground flat and smoothed to eliminate scratches incurred during the cutting process (Fig. 3(a)). Next, the cross-sections were painted black on the surface and covered with a fine-grade calcium carbonate powder (KSHG-20C). The pores, filled with white calcium carbonate paste, stand out prominently against the dark background of the cross-sections, previously painted black. Then, the cross-sections were scanned using a scanner with a resolution of 1200 dpi to obtain digital images of the cross-sections (see Fig. 3(b)). Using the *"imbinarize"* function in the program MATLAB^{TM} for the scanned images of the sample cross-sections to obtain the binary images of the sample cross-sections. In these binary images, the white portion represents the pore structure, while the black portion represents the remaining structural components of concrete (i.e., the cement paste and aggregates) (see Fig. 3(c)).

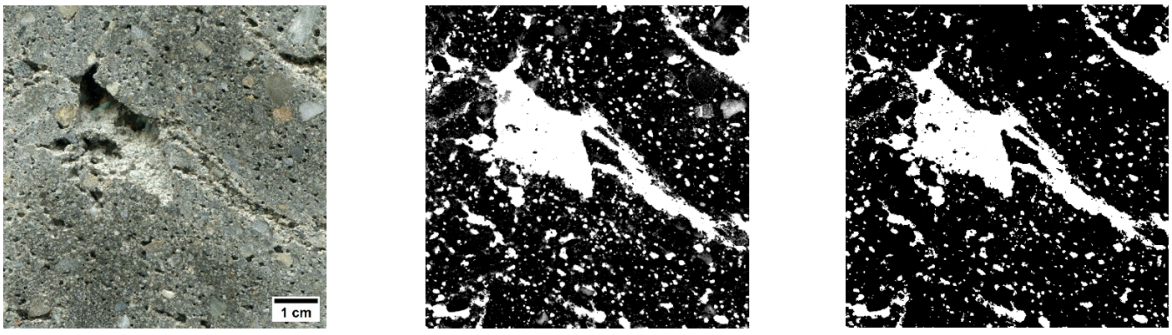

(a) Color scan image of the cross-section

(b) Color scan image of the cross-section after surface processing

(c) Binary image of the cross-section

Figure 3. An illustrative example of the image processing procedure to obtain a binary image of the pore structure within hardened concrete

4. Results and discussions

4.1. Analysis of ACF of the pore structure

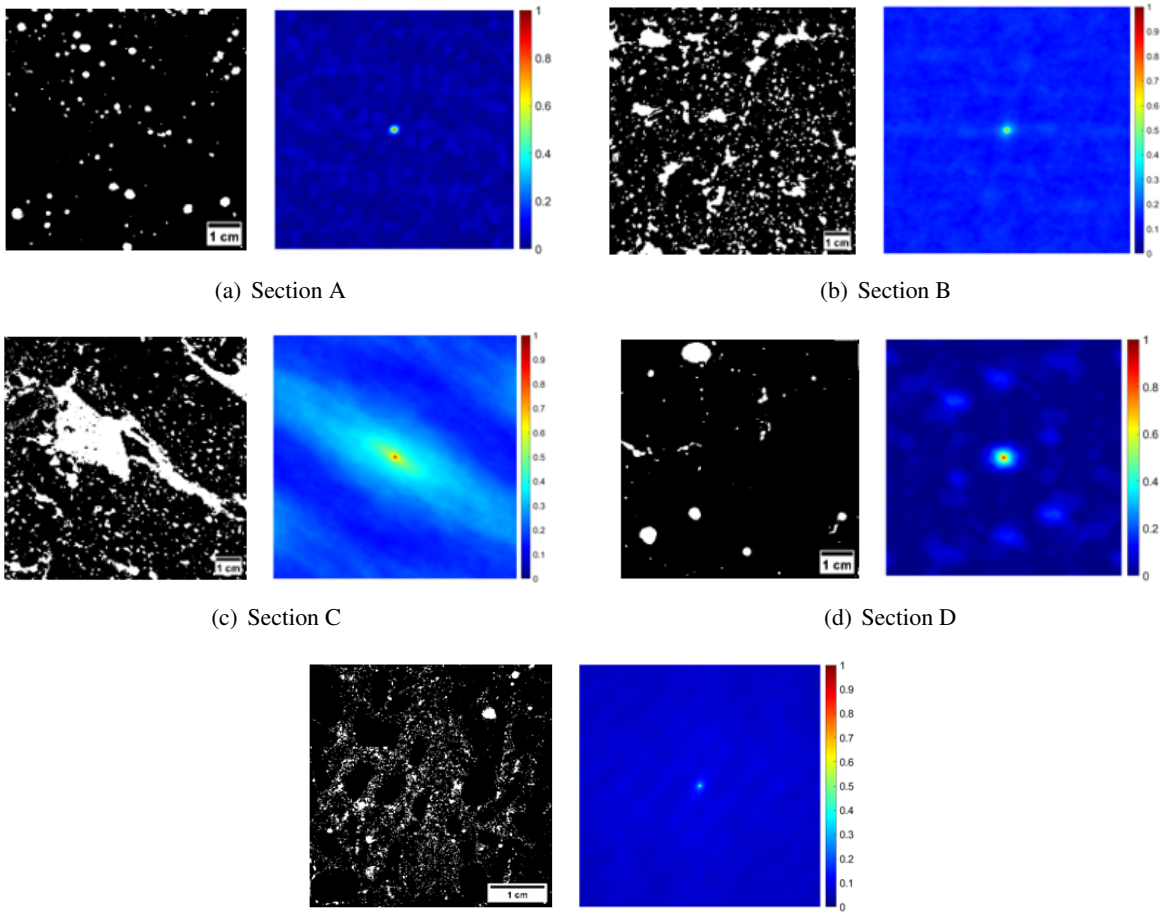

(a) Section A (b) Section B

(c) Section C (d) Section D

(e) Section E

Figure 4. Binary images of the cross-sections (left) and the corresponding digital images of ACF values (right)

Fig. 4 presents the binary images of the five cross-sections examined in this study and the digital images of the corresponding ACF values for those cross-sections. The ACF values shown in Fig. 4 have been normalized with the corresponding maximum ACF value on each image. As indicated in the figure, some noteworthy results are as follows:

- The ACF values reach their maximum at the symetric center of the image and gradually decrease in both directions to the stable value, which is ϕ_a, for all cross-sections. The area porosity, ϕ_a, is calculated by dividing the total area of the pore presented in the cross-section (i.e., the area of the white portion of the image; see Fig. 3(c)) by the entire area of the cross-sections. The values of ϕ_a for all five cross-sections are summarized in Table 1.

- The cross-sections with higher ϕ_a value will have correspondingly larger ACF values. As displayed in Fig. 4, the ACF values for all cross-sections examined in this study can be ordered as follows: C > B > A > E > D. This order aligns with the sequence of ϕ_a values reported in Table 1.

- In the matrix of ACF values (i.e., the right part of the graphs shown in Fig. 4), there exist two distinct regions: (i) the central region around the maximum ACF value, and (ii) the background region

with ACF values fluctuating around the ϕ_a value. The size of region (i) mainly depends on the size of the largest pore.

- The ACF values can indicate the distribution features of pores across the cross-section. Indeed, cross-sections A, B, and E have relatively even distributions of pores, resulting in corresponding ACF values also being evenly distributed in region (ii) (background region) (see Figs. 4(a), (b), (e)). Meanwhile, cross-sections C and D exhibit unevenly distributed pores, leading to an uneven distribution of ACF values in both directions (see Figs. 4(c), (d)).

- The shape of region (i) in the matrix of ACF values depends on the spatial distribution of pores across the cross-section. While cross-sections A, B, D, and E exhibit a relatively circular shape for region (i), that of cross-section C takes an elliptical shape with its major axis aligned with the primary orientation of its largest pore (see Fig. 4(c)). In other words, the ACF analysis enables the determination of the primary orientation of pore distribution across the cross-sections.

Table 1. Values of the area porosity (ϕ_a), the correlation length (X_0) and the characteristic size (l_0) for all the five examined cross-sections

Section	ϕ_a (%)	ACF		2PCF	
		X_0 (cm)	l_0 (cm)	X_0 (cm)	l_0 (cm)
A	3.3	0.162	0.001	0.147	0.001
B	14.9	0.375	0.007	0.515	0.007
C	21.2	1.307	0.011	2.270	0.027
D	2.6	0.365	0.002	0.292	0.002
E	7.6	0.792	0.006	1.021	0.006

4.2. Characteristic size of the pore structure

As mentioned in Section 2.3, the characteristic size of the pore structure is determined from the relationship between the correlation value (i.e. ACF or S_2 values) and the correlation distance (r). The variations of ACF and S_2 values with the distance r are displayed in Fig. 5(a) and Fig. 5(b), respectively. For all cross-sections, both ACF and S_2 values reach their maximum at ϕ_a, then gradually decrease and attain a stable value approximating ϕ_a^2 (expect for the S_2 value of cross-section C, see Fig. 5(b)). This result aligns with the theoretical principles of the ACF method, as illustrated in Fig. 2(b). As shown in Fig. 5, the rate of decrease in ACF and S_2 values with distance r primarily depends on the size of the pores appearing in the cross-sectional images, while being less influenced by the area porosity (ϕ_a). The decrease rate of the correlation function values can be quantified through the correlation length (X_0) (see Fig. 2(b) and Section 2.3).

Fig. 6 shows the variation of the X_0 and l_0 values determined through ACF and 2PCF in relation to the area porosity (ϕ_a) for all five cross-sections examined in this study. From this, a general trend is observed: as ϕ_a increases, both the values of X_0 and l_0 generally increase, regardless of cross-sections and correlation functions. Nevertheless, based on the obtained coefficient of determination (R^2) values (Fig. 6), it can be concluded that the correlation length (X_0) is less influenced by ϕ_a (with $R^2 < 0.7$). In contrast, ϕ_a has a significant impact on the characteristic size (l_0) (with $R^2 > 0.87$). In other words, the X_0 value only allows for a relative quantification of the pore size, but it cannot account for the porosity and shape of the pores, aspects effectively captured by the l_0 value. Consequently, the l_0 value is recommended to be used as the characteristic size for a comprehensive quantification of the pore structure of concrete.

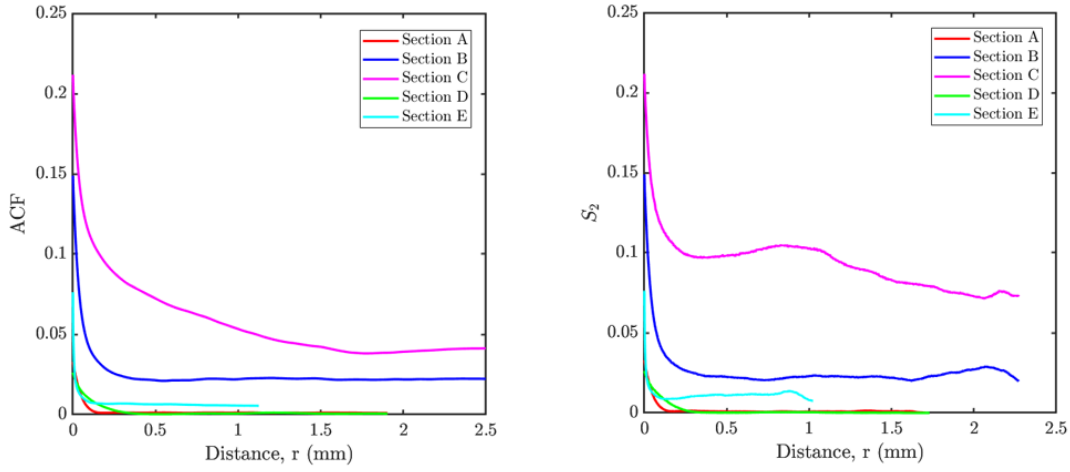

(a) ACF values vs. r (b) S_2 values vs. r

Figure 5. Variations of ACF and S_2 with the correlation distance, r, for all cross-sections.

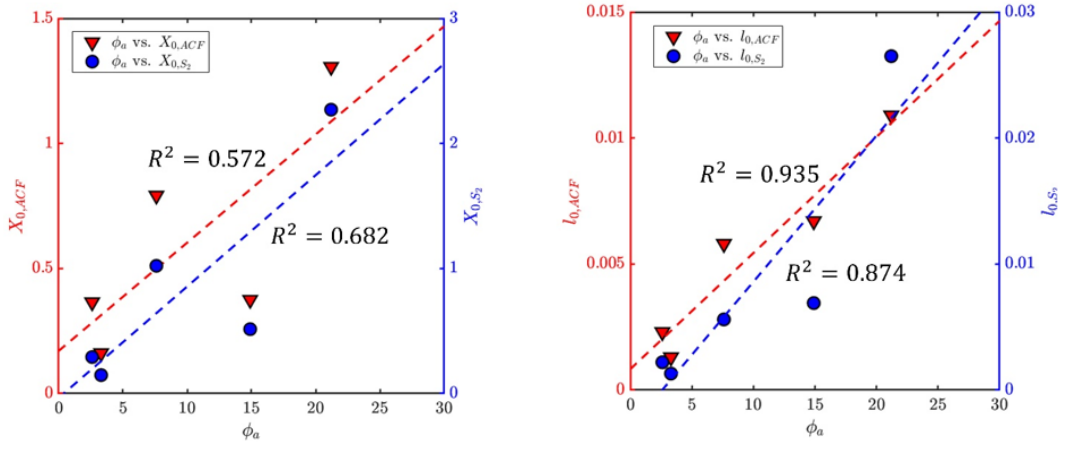

(a) X_0 vs. ϕ_a (b) l_0 vs. ϕ_a

Figure 6. Relationship between the X_0 and l_0 values determined through the ACF and 2PCF methods with the area porosity (ϕ_a) for all examined cross-sections

4.3. Comparison of ACF and 2PCF analysis results

Fig. 7(a) presents the relationship between the correlation length determined through the ACF method, $X_{0,ACF}$, and the corresponding values obtained from the 2PCF method, X_{0,S_2}. As shown in this figure and Table 1, most of the examined cross-sections have X_{0,S_2} values greater than $X_{0,ACF}$. With a coefficient of determination of $R^2 = 0.945$ (see Fig. 7(a)), it can be deduced that there is a linear proportion between these two correlation lengths as follows: $X_{0,S_2} \sim 1.6X_{0,ACF}$.

Fig. 7(b) shows a comparison of the characteristic size determined by the ACF method, $l_{0,ACF}$, with the corresponding values determined by the 2PCF method, l_{0,S_2}. Except for section C (with ϕ_a = 21.2%), the values of $l_{0,ACF}$ and l_{0,S_2} for the remaining four sections are highly similar. The significant difference between $l_{0,ACF}$ and l_{0,S_2} for section C can be explained as follows: the pore system of section C consists of interconnected airvoids forming the strips (see Fig. 4(c) left); consequently, the X_{0,S_2} value could be either the maximum distance between the pores or the largest size of the interconnected

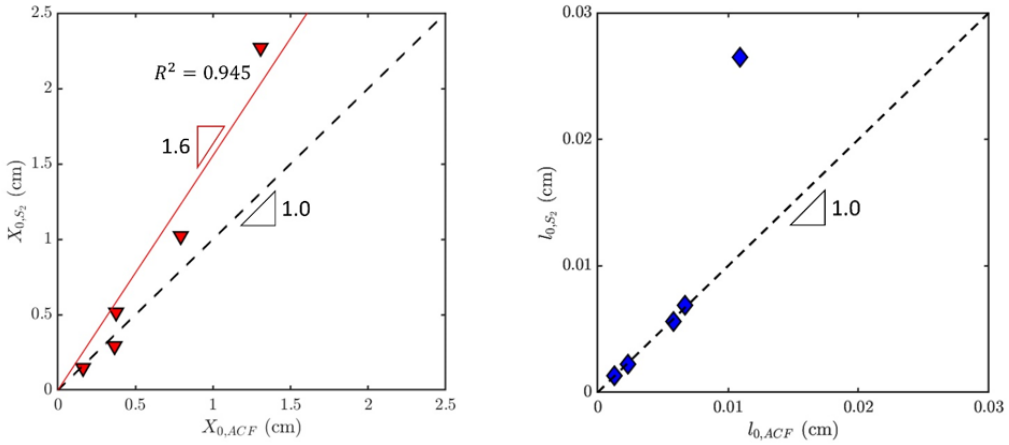

(a) $X_{0,ACF}$ vs. X_{0,S_2} (b) $l_{0,ACF}$ vs. l_{0,S_2}

Figure 7. Relationship between the values of $X_{0,ACF}$ and X_{0,S_2}, and $l_{0,ACF}$ and l_{0,S_2} for all the examined cross-sections

airvoid strips; on the other hand, the $X_{0,ACF}$ value is determined from the average of 360 ACF values corresponding to 360 rotation angles of the ACF matrix around the symmetry center (see Fig. 4(c) right); as a result, the X_{0,S_2} value of section C will be much larger than its $X_{0,ACF}$ value (see Table 1); furthermore, the ACF value for section C rapidly decreases with an increase in the correlation distance (r) (see Fig. 5(a)), while the S_2 value decreases at a slower rate, it even increases after decreasing at certain distances (see the S_2-value curve for section displayed in Fig. 5(b)); all these factors listed above contribute to the value of l_{0,S_2} for section C being much higher than its $l_{0,ACF}$ value.

From the similarity between the values of l_{0,S_2} and $l_{0,ACF}$ observed in this study, it can be concluded that, for concrete with an area porosity $\phi_a \leq 20\%$, the characteristic sizes of the pore structure determined by the ACF and 2PCF methods are similar. This, once again, allows for indicating that the characteristic size, l_0, calculated by Eq. (4) is an appropriate value for quantifying the pore structure of hardened concrete as a whole, instead of using the correlation length, X_0. On the other hand, this suggests that, for concrete with an area porosity $\phi_a > 20\%$, the characteristic size, l_0, should be determined using the ACF method, while the 2PCF method may yield inaccurate results. The main reason for this is that the S_2 values in this case offen do not converge to the value of ϕ_a^2 (see Fig. 5(b)). However, it is noteworthy that this finding was derived from only one cross-section with $\phi_a > 20\%$. Consequently, this conclusion needs further clarification through additional research similar to the present work, conducted on a large number of concrete cross-sections with $\phi_a > 20\%$. These additional works would, of course, be necessary to enable us to determine a threshold for the area porosity, beyond which the values of l_0 determined by the ACF and 2PCF methods are significantly different.

5. Conclusions

This paper has presented a comparative study of the autocorrelation function (ACF) and two-point correlation function (2PCF) methods applied to quantify the pore structure of concrete. From the obtained research results, several main conclusions can be highlighted, as follows:

- In terms of image analysis, the ACF provides a comprehensive and effective method to capture several factors, such as the porosity, the size and shape of the pores, and the spatial distribution of the pores when quantifying the pore structure of concrete, while the 2PCF only allows for the

quantification of the size and spacing of the pores. However, ACF requires the image of the cross-section to be square, whereas 2PCF can analyze images of any size and shape.

- For concrete with an area porosity ($\phi_a \leq 20\%$), the characteristic size of the pore structure of concrete, l_0, determined by both ACF and 2PCF methods, is highly similar.

- On average, the correlation length (X_0) estimated by the 2PCF method is more than 1.6 times greater than the corresponding value determined by the ACF method.

- The characteristic size (l_0) provides a more accurate and compressive quantitative measure of the pore structure of concrete than the correlation length (X_0).

Nevertheless, due to the limited number of cross-sections and the range of porosity considered in this study, similar research conducted on cross-sections with higher porosity would be necessary to determine the threshold at which the porosity significantly affects the analysis results of the ACF and 2PCF methods. Moreover, a comparative study between the results of analyzing the pore structure of concrete using the image analysis procedure presented in this paper and those obtained from other traditional experimental methods would be necessary to refine the findings of the present work.

References

[1] Monteiro, P. (2006). *Concrete: microstructure, properties, and materials*. Third edition, McGraw-Hill Publishing.

[2] Neville, A. M., Brooks, J. J. (2010). *Properties of concrete*, volume 4. Pearson Education Limited.

[3] Jakobsen, U. H., Pade, C., Thaulow, N., Brown, D., Sahu, S., Magnusson, O., De Buck, S., De Schutter, G. (2006). Automated air void analysis of hardened concrete — a Round Robin study. *Cement and Concrete Research*, 36(8):1444–1452.

[4] Igarashi, S.-i., Watanabe, A., Kawamura, M. (2005). Evaluation of capillary pore size characteristics in high-strength concrete at early ages. *Cement and Concrete Research*, 35(3):513–519.

[5] Das, B. B., Kondraivendhan, B. (2012). Implication of pore size distribution parameters on compressive strength, permeability and hydraulic diffusivity of concrete. *Construction and Building Materials*, 28(1): 382–386.

[6] Diamond, S. (2000). Mercury porosimetry. *Cement and Concrete Research*, 30(10):1517–1525.

[7] Zhao, H., Xiao, Q., Huang, D., Zhang, S. (2014). Influence of Pore Structure on Compressive Strength of Cement Mortar. *The Scientific World Journal*, 2014:1–12.

[8] Bhattacharjee, B., Kondraivendhan, B. (2010). Effect of age and water-cement ratio on size and dispersion of pores in ordinary portland cement paste. *ACI Materials Journal*, 107(2):147–154.

[9] Zingg, L., Briffaut, M., Baroth, J., Malecot, Y. (2016). Influence of cement matrix porosity on the triaxial behaviour of concrete. *Cement and Concrete Research*, 80:52–59.

[10] Gallé, C. (2001). Effect of drying on cement-based materials pore structure as identified by mercury intrusion porosimetry. *Cement and Concrete Research*, 31(10):1467–1477.

[11] Kumar, R., Bhattacharjee, B. (2004). Assessment of permeation quality of concrete through mercury intrusion porosimetry. *Cement and Concrete Research*, 34(2):321–328.

[12] Cook, R. A., Hover, K. C. (1999). Mercury porosimetry of hardened cement pastes. *Cement and Concrete Research*, 29(6):933–943.

[13] Diamond, S. (1971). A critical comparison of mercury porosimetry and capillary condensation pore size distributions of portland cement pastes. *Cement and Concrete Research*, 1(5):531–545.

[14] Mikhail, R. S., Copeland, L. E., Brunauer, S. (1964). PORE STRUCTURES AND SURFACE AREAS OF HARDENED PORTLAND CEMENT PASTES BY NITROGEN ADSORPTION. *Canadian Journal of Chemistry*, 42(2):426–438.

[15] Gonzalez, R. C., Woods, R. E. (2009). *Digital Image Processing*. Third edition, Pearson Education.

[16] Underwood, E. E. (1970). *Quantitative stereology*. Addison-Wesley Pub. Co.

[17] Falchetto, A., Moon, K., Wistuba, M. (2014). Microstructural Analysis and Rheological Modeling of Asphalt Mixtures Containing Recycled Asphalt Materials. *Materials*, 7(9):6254–6280.

[18] Moon, K. H., Falchetto, A. C., Jeong, J. H. (2014). Microstructural analysis of asphalt mixtures using digital image processing techniques. *Canadian Journal of Civil Engineering*, 41(1):74–86.
[19] Velasquez, R. A. (2009). *On the representative volume element of asphalt concrete with applications to low temperature*. University of Minnesota.
[20] Jiao, Y., Stillinger, F. H., Torquato, S. (2008). Modeling heterogeneous materials via two-point correlation functions. II. Algorithmic details and applications. *Physical Review E*, 77(3):031135.
[21] Heilbronner, R., Barrett, S. (2014). *Image Analysis in Earth Sciences: Microstructures and Textures of Earth Materials*. Springer Berlin Heidelberg.
[22] Kanit, T., Forest, S., Galliet, I., Mounoury, V., Jeulin, D. (2003). Determination of the size of the representative volume element for random composites: statistical and numerical approach. *International Journal of Solids and Structures*, 40(13–14):3647–3679.
[23] Baniassadi, M., Ahzi, S., Garmestani, H., Ruch, D., Remond, Y. (2012). New approximate solution for N-point correlation functions for heterogeneous materials. *Journal of the Mechanics and Physics of Solids*, 60(1):104–119.
[24] Heilbronner, R. (2002). Analysis of bulk fabrics and microstructure variations using tesselations of autocorrelation functions. *Computers & Geosciences*, 28(4):447–455.
[25] Pfleiderer, S., Ball, D. G. A., Bailey, R. C. (1993). AUTO: A computer program for the determination of the two-dimensional autocorrelation function of digital images. *Computers & Geosciences*, 19(6): 825–829.
[26] Heilbronner, R. P. (1992). The autocorrelation function: an image processing tool for fabric analysis. *Tectonophysics*, 212(3–4):351–370.
[27] Cong, V. C. (2023). Simplified approach for quantitative analysis of hardened concrete microstructure using autocorrelation function. *Journal of Science and Technology in Civil Engineering (STCE) - HUCE*, 17(4):66–79.
[28] Torquato, S. (1991). Random Heterogeneous Media: Microstructure and Improved Bounds on Effective Properties. *Applied Mechanics Reviews*, 44(2):37–76.
[29] Berryman, J. G. (1985). Measurement of spatial correlation functions using image processing techniques. *Journal of Applied Physics*, 57(7):2374–2384.
[30] Kanit, T., N'Guyen, F., Forest, S., Jeulin, D., Reed, M., Singleton, S. (2006). Apparent and effective physical properties of heterogeneous materials: Representativity of samples of two materials from food industry. *Computer Methods in Applied Mechanics and Engineering*, 195(33–36):3960–3982.
[31] Cannone Falchetto, A., Moon, K. H. (2015). A novel micromechanical–analogical model for low temperature creep properties of asphalt binder and mixture. *Canadian Journal of Civil Engineering*, 42(12): 1019–1031.